

**PROCEEDINGS OF THE THIRD CONFERENCE
LOCALIZATION & ENERGY TRANSFER IN NONLINEAR
SYSTEMS**

EDITORS

LUIS VÁZQUEZ

Universidad Complutense and Centro de Astrobiología CSIC/INTA, Spain

ROBERT S. MACKAY

Warwick University, UK

MARIÁ PAZ ZORZANO

Centro de Astrobiología CSIC/INTA, Spain

WORD SCIENTIFIC

New Jersey • London • Singapore • Hong Kong

COPYRIGHT © 2003, ISBN 981-238-296-8

pp 68-101

**EXPERIMENTAL STUDIES AND THEORY OF
NONLINEAR ROTATIONAL DYNAMICS IN THE
QUANTUM REGIME: THE INTERPLAY OF STRUCTURE,
DYNAMICS AND LOCALIZATION IN CRYSTALS**

FRANÇOIS FILLAUX AND BÉATRICE NICOLAÏ

*LADIR-CNRS and Université Pierre et Marie Curie
2 rue H. Dumant, 94320 Thiais, France
E-mail: fillaux@glvt-cnrs.fr*

ALAIN COUSSON

*Laboratoire Léon Brillouin (CEA and CNRS)
CEA Saclay, 91 191, Gif sur Yvette cedex, France
E-mail: cousson@llb.saclay.cea.fr*

Experimental and theoretical studies of quantum rotation of methyl groups in crystals are presented. Tunnelling spectroscopy with the inelastic neutron scattering technique and determination of angular probability densities of methyl groups in their rotational planes with the single crystal neutron diffraction technique are introduced. The importance of temperature and deuteration effects is emphasized. Three examples are presented. i) In the manganesediacetate tetrahydrate crystal, $\text{Mn}(\text{CH}_3\text{COO})_2 \cdot 4\text{H}_2\text{O}$, methyl groups are in three different environments, their rotational axes have different orientations and they are well separated from each other. They can be regarded as isolated single rotors and tunnelling excitations are localized. ii) In the lithiumacetate dihydrate crystal, $\text{CH}_3\text{COOLi} \cdot 2\text{H}_2\text{O}$, all methyl groups are equivalent. Close-contact pairs of face-to-face methyl groups are distributed in a nearly hexagonal planar structure with rather short methyl-methyl distances. The face-to-face methyl groups twisted by 60° perform combined rotation represented with symmetry adapted coordinates. Ordering of the methyl groups at a low temperature upon deuteration reveals significant interaction between pairs. However, in the 2D structure arising from methyl-methyl interaction there is no evidence for collective rotation of the pairs. Tunnelling excitations are localized within pairs. iii) In the 4-methylpyridine ($\text{C}_6\text{H}_7\text{N}$) crystal the distances between methyl groups are quite similar to those in lithiumacetate. However, in the tetragonal structure, the face-to-face methyl groups twisted by 90° to each other cannot perform combined rotation. The corresponding effective potential is virtually a constant. There is no phase transition upon methyl deuteration. Methyl groups form orthogonal infinite chains parallel to a or b and virtually isolated from each other. The collective rotation in 1D is represented in the dispersive regime with the quantum sine-Gordon theory. Tunnelling transitions are represented with extended states in an energy-band structure. Additional transitions are attributed to travelling states of a dimensionless pseudo particle: the quantum breather mode. All excitations are totally delocalized.

1. Introduction

Light particles moving in a potential with topological degeneracy manifest their quantum nature *via* tunnelling, one of the evidences of the profound difference between classical and quantal worlds. Owing to the spatial extension of the wave function, the degenerate ground state in the classical regime splits into sublevels. In the condensed matter, the observation of tunnelling sheds light onto fundamental problems of quantum mechanics in a complex environment.

For light quantum rotors like methyl groups, the topological degeneracy arises from the intrinsic periodicity of the angular coordinate and rotational tunnelling is observed in many crystals at a low temperature.¹ The upper limit of the tunnel splitting is the rotational constant $B = \hbar^2/2I_r$, where I_r is the moment of inertia of the rotor. For an isolated and rigid CH_3 group rotating around its axis of inertia supposed to be fixed, B ranges from 0.650 to 0.700meV and from 0.325 to 0.350meV for the deuterated analogue CD_3 . The magnitude of the tunnel splitting depends on the particle mass and potential shape (distances between identical sites, barrier height...). Deuteration is of dramatic consequence to the tunnelling frequency.

In many molecular crystals the frequency range for tunnelling is well separate from the density-of-states for optical phonons and dynamical interaction with the lattice is very weak. Tunnelling transitions are specific to the rotational coordinates and can be represented with a rather simple Hamiltonian. Therefore, rotational tunnelling is unique to observing non-linear dynamics in the quantum regime. For example, quantum rotation of isolated rotors can be regarded as the solution of the Mathieu equation at the molecular level (see below section 2).² Energy localization is characteristic of these tunnelling transitions.^{3,4} For some systems, methyl-methyl interaction may compete with localization. For example, the rotational dynamics in the lithiumacetate dihydrate crystal are solutions of the non-linear and nonintegrable Hamiltonian for coupled pairs of rotors (see below section 3).^{5,6,8,7,9} Tunnelling excitations remain largely localized in pairs. Finally, collective rotational dynamics in the 4-methylpyridine crystal are solutions of the sine-Gordon Hamiltonian in the quantum regime (see below section 4).^{10,11,12,13,14,16,15} Tunnelling excitations are totally delocalized

For methyl groups, the great specificity of rotational tunnelling can be fully exploited with the inelastic neutron scattering (INS) technique, because the cross-section of H atoms for incoherent neutron scattering is much greater than for any other atom, by about one order of magnitude.¹⁷ Any intensity arising from the crystal density-of-states (primarily acoustic

phonons in the tunnelling energy range) can be ignored.

Nowadays, transitions above $\approx 1\mu\text{eV}$ are observed with advanced spectrometers available at various neutron sources. However, the observation of tunnelling transitions for deuterated analogues is hampered by the much weaker cross section of D atoms and by the dramatic decrease of the splitting upon deuteration. This information is often missing and this is a limitation for modelling rotational dynamics.

Pioneering INS works with rather modest resolution have first revealed single tunnelling transitions and dynamical models for single rotors were sufficient to interpreting the spectra.^{3,4} With better spectrometer resolution, multi-component spectra due to dynamical coupling were observed and different models were proposed to account for local or collective rotational dynamics. The diversity of models is partly due to the lack of information and this is a long lasting source of polemics that keep the field lively. Unfortunately, the hope that advanced methods of quantum chemistry and molecular dynamics simulation could provide realistic modelling of the effective potentials experienced by methyl rotors is not yet realized.^{18,19} As long as tunnelling frequencies cannot be calculated with good accuracy (say a few μeV), experiments remain the best source of knowledge of these quantum dynamics. This is a strong incentive to undertaking new experiments in order to remove ambiguities, as much as possible. Studies of various isotope derivatives and mixtures, tunnelling spectra measured on single crystals, determination of the angular probability density and of the kinetic momentum distribution are among the salient progresses which have shed a new light on quantum rotation in solids, during the last decade, or so.

This paper is meant to be an introduction to tunnelling spectroscopy with neutrons and to the analysis of model Hamiltonians for quantum rotation. We present three prototypical examples of quantum rotors with totally different dynamics. The impact of advanced techniques and data analysis to theoretical developments is emphasized. We hope to convince the reader that rotational dynamics of methyl groups is a unique benchmark for quantum mechanics in the solid states. Moreover, this field of investigation is a lively forum for experimental chemists/physicists on the one hand and theoreticians/mathematicians, on the other. To launch fruitful collaborations between such experts from different fields is a major goal of the LOCNET network.

2. The single methyl rotor

The simplest model for methyl rotation is the single rigid rotor in a threefold potential. The Hamiltonian

$$H_1 = -B \frac{\partial^2}{\partial \theta^2} + \frac{V_{03}}{2} (1 - \cos 3\theta) \quad (1)$$

can be transformed into a Mathieu equation.² Eigen states $E_{n\sigma}$ and wave functions $\Psi_{n\sigma}(\theta)$ depend on two quantum numbers: the principal torsional quantum number n for the oscillator limit with full degeneracy and a sub-level index σ , which gives the symmetry of the wave function. As there is no analytical solution for the eigen values, numerical calculations using the basis set of the free rotor are carried out with the variational method (Figure 1).²⁰ In this simple model, there is only one tunnelling transition and it is straightforward to estimate threefold potential barriers from measurements. As the tunnel splitting varies practically exponentially with the potential barrier, tunnelling is a very sensitive probe of the local potential experienced by methyl groups in crystals. Experimental values can be compared with those estimated with various models (for example quantum chemistry methods).^{18,19}

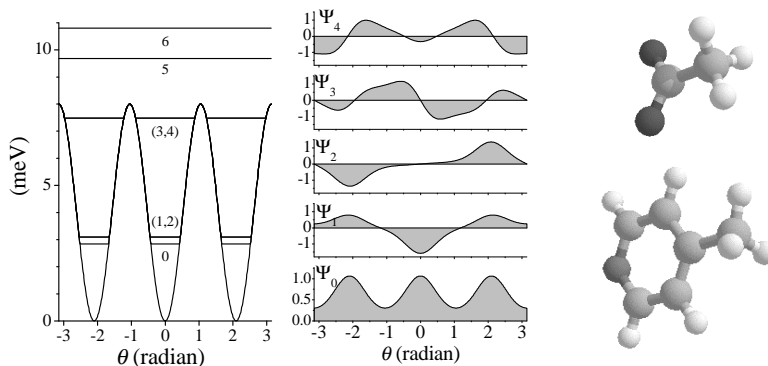


Figure 1. Schematic representation of the eigen states and eigen functions for a methyl rotor in a threefold potential and molecular models for the acetate entity (upper) and 4-methylpyridine (lower).

The effective potential can be decomposed into an internal potential that is determined by the molecular frame bearing the methyl group and an external contribution arising from the environment. As internal barriers are negligible for the acetate entity and for the 4-methylpyridine molecule

(see Figure 1), the observed potential barriers are entirely due to the environment and can be tentatively related to the crystal structure.

A tutorial example is the crystal of manganese diacetate tetrahydrate, $\text{Mn}(\text{CH}_3\text{COO})_2 \cdot 4\text{H}_2\text{O}$, which contains 3 crystallographically inequivalent methyl groups.²¹ The INS spectrum of a powdered sample at 1.5 K reveals 3 tunnelling transitions at 1.2, 50 and 137 μeV , with equal intensities.²² The corresponding potential barriers (49.0, 17.5 and 11.5 meV, respectively) emphasize the great sensitivity of the tunnelling frequency to the local potential. However, effective potentials arising from the crystal environment at each site are sums of many contributions (atom...atom, electrostatic, multipolar...) that are poorly known and cannot be calculated with good accuracy. Unavoidable uncertainty precludes a firm assignment scheme for the tunnelling frequency at each rotor site.

2.1. INS spectra of oriented single crystals

The diffraction techniques are used to determine crystal structures with great accuracy. For ordered crystal rather sharp spots of intensity (Bragg-peaks) are observed for well defined orientations of the crystal and detector with respect to the incident beam. The diffraction pattern defines the reciprocal lattice that is a Fourier transformation of the direct lattice. The intensity of the peaks is determined by the lattice symmetry and the scattering cross-section of the atoms at each site.

X-ray diffraction is the most used technique available in many laboratories as a routine facility. The intensity scattered by atoms increases with the number of electrons. Consequently, the Bragg-peak intensities are largely dominated by contributions from heavy atoms whilst hydrogen atoms can be totally hidden. As a general rule, hydrogen atoms of methyl groups cannot be localized accurately with X-ray. However, the crystal structure is a source of information regarding the environment of the methyl groups.

For example, the structure of manganese diacetate tetrahydrate determined with X-ray reveals the orientations of the rotational axes of the methyl groups (see Figure 2).^{23,24,25} Then, with properly oriented single crystals, the INS intensity of the tunnelling transitions can be probed as a function of the orientation of the momentum transfer vector \mathbf{Q} with respect to the rotational axes. ($\mathbf{Q} = \mathbf{k}_0 - \mathbf{k}_f$ with $|\mathbf{k}_0| = 2\pi/\lambda_0$ and $|\mathbf{k}_f| = 2\pi/\lambda_f$, where λ_0 and λ_f are the incident and scattered wavelengths, respectively.) The intensity is a maximum when \mathbf{Q} is perpendicular to the axis of rotation and it vanishes if \mathbf{Q} is parallel. According to such measurements, the tunnelling frequencies at 1.2, 50 and 137 μeV are attributed to sites C, B

and A, respectively.

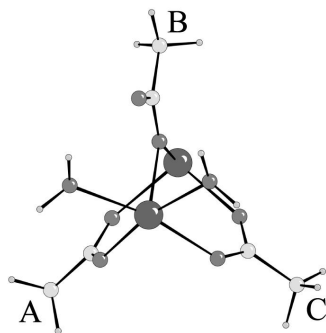


Figure 2. Schematic representation of the arrangement of the three inequivalent methyl groups in the manganediacetate tetrahydrate crystal at 14 K, after ref. 21

2.2. The density probability of methyl rotors

The neutron diffraction technique is complementary to X-ray diffraction. The scattering cross section of electrons is negligible and Bragg-peaks arise from scattering by nuclei. This technique is unique to determine the position of H-atoms because the nuclear cross-sections are on the same order of magnitude for all nuclei. For example, the orientation of the methyl groups and of the water molecules were determined for manganediacetate tetrahydrate (see Figure 2).²¹

With the Fourier difference method, data obtained from single-crystal neutron diffraction provide a full view of the probability density of the H(D)-atoms. For this purpose, once the crystal structure has been determined, Bragg-peak intensities can be calculated for an ideal crystal in which the scattering cross section of the H(D)-atoms of the methyl groups is set to zero. The difference from the original pattern contains specific information on the methyl H(D)-atoms. Further Fourier back-transformation gives the probability density distribution in direct space (for example, see Figure 3).

Because diffraction arises from coherent scattering by a large number of atoms in a regular lattice, disorder appears as a perturbation of the lattice periodicity averaged over space and time. It is impossible to distinguish statistical and dynamical disorder. However, the dynamical orientational disorder of methyl group is so large compared to disorder arising from other vibrations that the angular probability density is quite representative of the wave function and can be somehow related to the potential.

2.2.1. Methyl rotors at low temperature

The Fourier difference maps for the three methyl groups in the manganese-diacetate tetrahydrate crystal at 14 K are presented in Figure 3. The

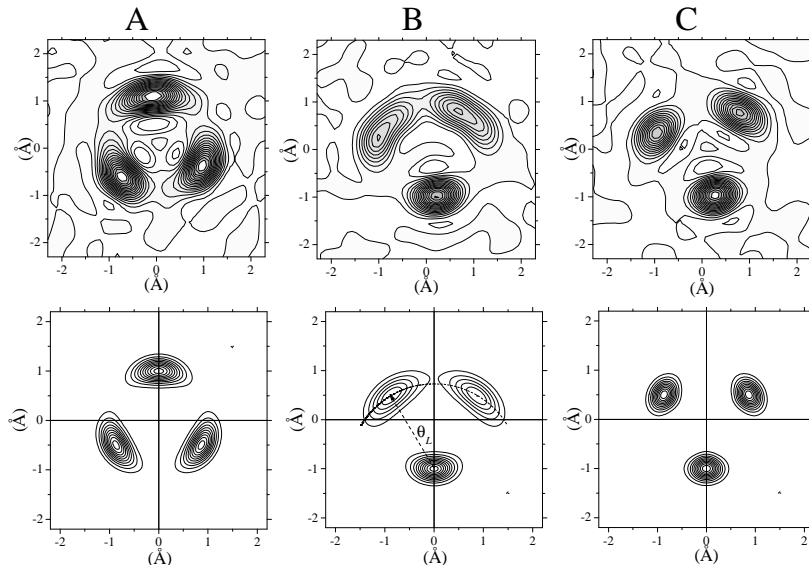


Figure 3. Top: measured probability density distributions for the three inequivalent methyl groups in the manganese diacetate tetrahydrate crystal measured at 14 K, after ref. 21. Labels A, B and C refer to those in Figure 2. Bottom: calculated maps (see text). A: $V_3 = 11.5$ meV, $u_r^2 = 0.05$ Å². B: $V_3 = 17.6$ meV, $u_r^2 = 0.05$ Å², $\theta_L^2 = 0.06$ rad². C: $V_3 = 49.0$ meV, $u_r^2 = 0.05$ Å².

different dynamics are immediately recognized by visual examination. The highest potential barrier (lowest tunnelling frequency) occurs for the methyl group C whose protons are quite localized. The more delocalized protons for the methyl group A correspond to the lowest potential barrier (highest tunnelling frequency).

The map for the methyl group B is much more intriguing. Whereas the distributions for A and C have clearly the threefold symmetry anticipated for rigid methyl groups with fixed axes, the probability densities at the three proton sites are quite different for methyl B. Of course, as each proton is totally delocalized the total probability is the same for each site. The probability density is actually a comprise of several contributions arising from both the methyl groups and the crystal lattice. It is necessary to analyze these maps more thoroughly in order to highlight the rotational

dynamics.

One can distinguish three contributions to the probability density: (*i*) the rotational dynamics; (*ii*) the deformation of the methyl groups due to internal vibrations; (*iii*) the lattice dynamics and/or disorder. Because the tunnelling occurs at a very low frequency, lattice dynamics and internal vibrations can be represented with time/space-averaged distributions. It is convenient to distinguish isotropic and anisotropic contributions. The former, as opposed to the latter, does not disturb the threefold symmetry.

i) From the tunnelling frequency and Eq. (1) the temperature dependent angular probability density is determined by the Boltzmann distribution:

$$P_d(\theta, T) = \frac{\sum_{n\sigma} \Psi_{n\sigma}^2(\theta) \exp(-E_{n\sigma}/kT)}{\sum_{n\sigma} \exp(-E_{n\sigma}/kT)} \quad (2)$$

ii) Methyl groups are not perfectly rigid. The 8 degrees of freedom for internal motions give rise to complex vibrations that can be represented with a static distribution for the H-atoms. The projection onto the rotational plane gives an isotropic distribution with a Gaussian like profile. The variance (mean-square amplitude) of $\approx 0.01 \text{ \AA}^2$ is largely temperature independent.

iii) Similarly, lattice vibrations give rise to an isotropic Gaussian distribution for the C-atom with a variance of $\approx 0.02 \text{ \AA}^2$ at a low temperature. This value may increase significantly as the temperature is closer to the melting point. The mean square displacements in the rotational plane are further multiplied by a factor of ≈ 2 due to the distance between the rotational plane and the C-atom.

All together, the isotropic mean square displacement due to vibrations $u_{iso}^2(T)$ is $\approx 0.05 \text{ \AA}^2$ at a low temperature and the observed angular distribution is a convolution:

$$P(\theta, T) = P_d(\theta, T) \otimes \rho_\varphi(\varphi - \theta, T); \quad (3)$$

with

$$\rho_\varphi(\varphi, T) = \left(\frac{1}{\pi \varphi_{iso}^2(T)} \right)^{\frac{1}{2}} \exp \left[-\frac{(\varphi - \theta)^2}{\varphi_{iso}^2(T)} \right] \quad (4)$$

where $\varphi_{iso}^2(T) = u_{iso}^2(T)/r^2$. The rotational radius for protons r is $\approx 1 \text{ \AA}$. The radial distribution is gaussian in shape and can be represented as:

$$\rho_r(r, T) = \left(\frac{1}{\pi u_{iso}^2(T)} \right)^{\frac{1}{2}} \exp \left[-\frac{(r - r_0)^2}{u_{iso}^2(T)} \right]. \quad (5)$$

With this rather simple model, it transpires that the probability densities measured for the A and C rotors are directly related to the square of the rotational wave functions, with minor contribution from other internal and lattice dynamics (see Figure 3).

For the B rotor, the dynamical probability density is convoluted with an anisotropic distribution of the angular coordinate θ_L representing the orientational disorder of the methyl axis with respect to one of the potential minima. The physical picture emerging from this map is quite unforeseen. In the effective potential $V(\theta_L)$, the slow methyl rotational is quenched, one of the minima is much deeper at one proton site than at the others. Indeed, this is not in conflict with the threefold symmetry of the effective rotational potential $V_{03}(\theta)$ averaged over the fast lattice coordinate θ_L .

2.2.2. Methyl rotors at room temperature

Tunnelling bands are well observed only at very low temperature, usually below 50 K. At higher temperatures, bandwidths increase and transitions merge into the huge peak for elastic scattering. The prevailing interpretation is that the quantum dynamics switches to classical diffusion at high temperature. Nowadays, density distributions obtained at any temperature compatible with the stability of the crystal shed light onto the rotational dynamics at high temperature.

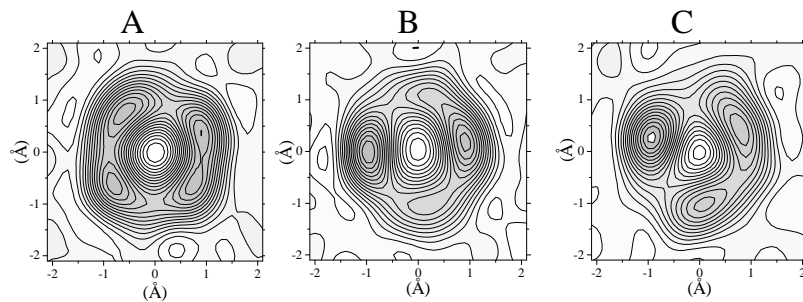


Figure 4. Measured probability density distributions for the three inequivalent methyl groups in the manganese diacetate tetrahydrate crystal at 300 K after ref. 21. Labels A, B and C refer to those in Figures 2 and 3.

At room temperature, the proton distributions for rotors A and B are almost isotropic (see Figure 4). Nearly free rotation arises mainly from thermal population of rotational levels close to, or above, the top of the potential barrier (see Figure 1). (The rather modest anisotropic features

may arise from convolution with lattice displacements.) For the C rotors, partial localization of the protons due to hindered rotation is still observed and the effective potential barrier still exists at 300 K. In addition, a marked anisotropic contribution from the lattice dynamics is observed. The quantum dynamics is likely to survive even at room temperature and mixing of higher rotational states with phonons may take place.

3. Quantum rotational dynamics for pairs of coupled rotors

In the lithiumacetate dihydrate ($\text{CH}_3\text{COOLi}\cdot 2\text{H}_2\text{O}$ or Liac- h_7) crystal the rotational dynamics is better represented with pairs of coupled methyl groups.

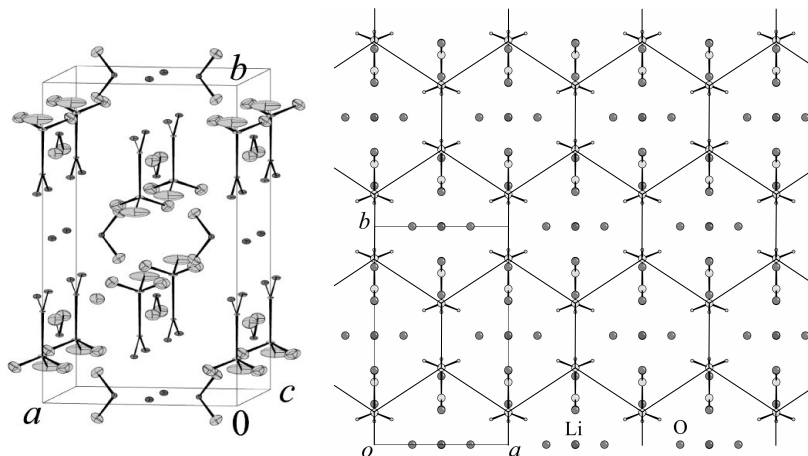


Figure 5. Crystal structure of the methyl deuterated lithium acetate dihydrate after ref. 26. Left: view of the unit cell with thermal ellipsoids. Right: projection onto the (a, b) plane. The lines along nearest neighbor interactions are guides for eyes. For the sake of clarity, the hydrogen atoms of the water molecules are hidden.

3.1. A honey comb network in 2D of quantum rotors

For the fully hydrogenated derivative the crystal symmetry ($Cmmm$) remains unchanged upon cooling from room temperature down to 1 K.^{27,19} The methyl groups are arranged in infinite chains, along the a crystal axis, of face-to-face coaxial pairs parallel to b (see Figure 5). The distances be-

tween consecutive axes of rotation ($a/2 \approx 3.4\text{\AA}$) and between the methyl-carbon atoms within pairs ($0.3b \approx 3.3\text{\AA}$) are significantly shorter than the van der Waals radii and significant interactions along the chains and within pairs are schematically represented as a honey comb like structure in 2D, parallel to the (a, b) planes. The inter-layer distances of $\approx 6.56\text{\AA}$ between (a, b) planes are much greater and interactions between methyl groups along the c axis is negligible.

3.2. A phase transition induced by methyl deuteration

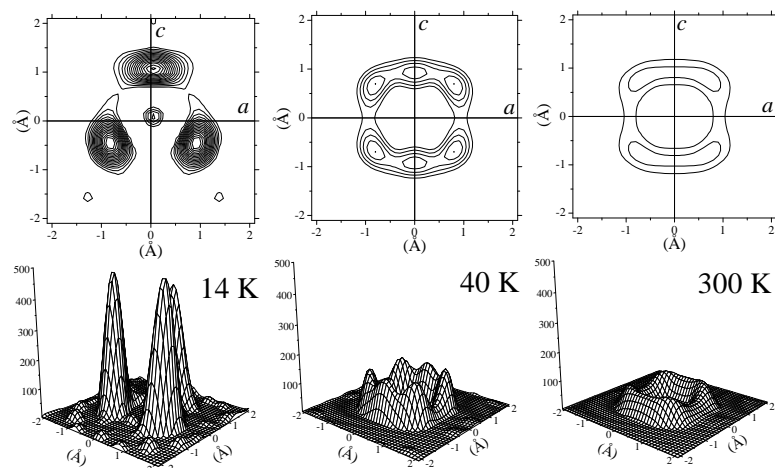


Figure 6. Probability density distributions of the deuterium atoms in the methyl deuterated lithium acetate dihydrate ($\text{CD}_3\text{COOLi}\cdot 2\text{H}_2\text{O}$) after ref. 26: at 14 K in the ordered phase $Pman$, at 40 K in the $Cmmm$ phase, slightly above the transition, and, in the same phase, at room temperature.

For $\text{Liac-}h_7$ the methyl groups are totally disordered at any temperature and the angular probability density is totally isotropic, even at $\approx 1\text{ K}$.¹⁹ Quite surprisingly, the methyl deuterated derivative ($\text{CD}_3\text{COOLi}\cdot 2\text{H}_2\text{O}$ or $\text{Liac-}d_3h_4$) undergoes a phase transition at 17.5 K, from $Cmmm$ to $Pman$ symmetry. The ordering of the centrosymmetric pairs of methyl groups is clearly observed with the neutron diffraction technique (Figure 5).^{28,26} As all other atomic coordinates remain virtually unchanged, there is no significant variation of the effective potential arising from heavy atoms and the phase transition is entirely due to mass effects on the quantum dynamics.

In the ordered phase at 14 K the localization of the probability density

distribution (Figure 6) is consistent with a rather high potential barrier. The two methyl groups in centrosymmetric pairs are indistinguishable and their images are superimposed in the Fourier difference. (The three peaks do not mean that the two methyl groups are in the eclipsed conformation.) At 300 K, the disorder is fully established. At 40 K, there is a mixture of ordered and disordered methyl groups which means that the potential barrier does not vanish at the phase transition. The density is a superposition of angular distributions for delocalized ($\approx 50\%$) and localized deuterium atoms ($\approx 50\%$). The six maxima do not mean that the rotational potential changes progressively from threefold to sixfold symmetry and then to free rotation upon increasing the temperature. At 40 K deuterium atoms are still partially ordered but face-to-face methyl groups are no longer indistinguishable in the $Cmmm$ phase.

3.3. The tunnelling spectrum

Early measurements of the proton spin-lattice relaxation have revealed almost free rotation of the methyl groups.²⁹ However, the tunnelling bands observed in the 0.3 meV range (see Figure 7) are quite below the frequency anticipated for almost free rotation. Moreover, since all methyl groups in the crystal experience the same effective potential the rather complex spectrum must be interpreted in terms of dynamical correlation between indistinguishable quantum rotors.

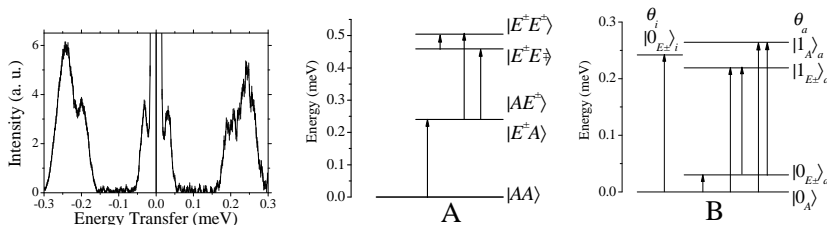


Figure 7. Left: the INS tunnelling spectrum of lithium acetate dihydrate at 1.5 K. Right: energy level schemes for a pair of coupled rotors with fixed parallel axes (see text), according to ref. 5 (A) or ref. 26 (B).

In the low-resolution limit, the threefold potential barrier for a single transition at $\approx 0.240\text{meV}$ in Eq. (1) is about 8 meV. Simple examination of Figure 1 reveals that the proton density should be quite localized at a low temperature. This is in conflict with the full delocalization experimentally observed.

For the CD₃ derivative the tunnelling frequency calculated at 33μeV with the same potential barrier is actually observed at 12.5μeV.⁶ Apparently, there is a significant increase of the effective barrier to ≈ 11.6meV. This may contribute to the ordering of the CD₃ at low temperature (see below section 3.7).

3.4. The coupled pair model

The single rotor is clearly unable to account for the complexity of the observed spectrum. Coupled rotation of pairs of methyl groups with parallel axes suggested by the crystal structure was first represented with the Hamiltonian depending on the angular coordinates θ_1 and θ_2 :^{7,6}

$$H_2 = -B \left(\frac{\partial^2}{\partial \theta_1^2} + \frac{\partial^2}{\partial \theta_2^2} \right) + \frac{V_{03}}{2} \cos 3\theta_1 + \frac{V_{03}}{2} \cos 3\theta_2 + \frac{W_{12}}{2} \cos 3(\theta_1 - \theta_2) \quad (6)$$

Each top experiences the same on-site potential V_{03} and the coupling depends only on the phase difference of the two rotors. In contrast to the textbook case of coupled harmonic oscillators, this Hamiltonian cannot be diagonalized by simple transformation into normal coordinates.⁹ On the other hand, numerical calculation of the eigen states and eigen functions requires very large basis sets with dimension N^2 , where N is the size of the basis set for each rotor. Early calculations carried out with a very limited basis sets ($N = 9$)⁷ were certainly lacking of accuracy and deserve some reservations. Furthermore, as symmetric and antisymmetric states are no longer separate, the interpretation of the energy level scheme is quite cumbersome.

In order to analyze Eq. (6) the potential terms were ignored ($V_{03} = W_{12} = 0$) and energy levels were distinguished according to their symmetry: the ground state (A_1A_2 at $E = 0$), first excited states corresponding to the transfer of one quantum to one of the two tops ($E_1^\pm A_2$ and $A_1 E_2^\pm$ at $E = B$) and higher states corresponding to the transfer of one quantum to each top ($E_1^\pm E_2^\pm$ and $E_1^\pm E_2^\mp$ at $E = 2B$).⁷ Then, the energy level scheme for non-zero potential terms was obtained by continuation of the zero-potential limit. It was concluded that AE^\pm states should occur in all cases (see Figure 7A). However, according to basic quantum mechanics for two coupled and indistinguishable rotors, AE^\pm states are not eigen states. This speculation is certainly an error and leads to misinterpretation of the spectrum. According to the energy level scheme in Figure 7A, the INS spectrum was decomposed into four components at 0.283, 0.250, 0.214 and 0.030 meV. The estimated values (namely $V_{03} \approx 7.6$ meV and $W_{12} \approx -17.0$ meV)⁶ are totally in conflict with the crystal structure.

Firstly, the on-site potential barrier quite similar to that for the single rotor must be rejected. Secondly, the negative value for W_{12} favors the eclipsed configuration ($\theta_1 = \theta_2$), whereas the crystal structure shows the staggered configuration for face-to-face methyl groups at low temperature (see Figure 5). (It is unlikely that the eclipsed configuration would be favored only for the hydrogenated methyl groups.) Thirdly, we are not able to confirm these calculations. Finally, among the 4 transitions predicted in Figure 7A, three of them are hot transitions and their intensities should decrease at a low temperature. At 1.5 K the relative populations of the $|AE\rangle$ level at $\approx 0.250\text{meV}$ and $|EE\rangle$ levels at $\approx 0.500\text{meV}$ should be $\approx 710^{-2}$ and $\approx 510^{-3}$ respectively. Therefore, the spectrum should be largely dominated by the single $|AA\rangle \rightarrow |AE\rangle$ transition. However, this is not confirmed by experiments.⁸

3.5. Symmetry adapted coordinates

In order to propose a more rigorous analysis of the dynamics of coupled pairs, it is necessary to pay attention to the crystal structure in which the face-to-face methyl groups are indistinguishable and form centrosymmetric pairs. Consequently, the dynamics are better represented with symmetry-adapted coordinates corresponding to in-phase $\theta_i = (\theta_1 + \theta_2)/2$ and anti-phase $\theta_a = (\theta_1 - \theta_2)/2$ rotation. In contrast, again, to the harmonic case, the choice of the symmetry adapted coordinates is much more constrained. It is imposed by the periodicity of the rotors. The coordinates must be compatible with the threefold and sixfold periodicity for in-phase and anti-phase rotation. Any change of the periodicity would give a totally different energy level scheme.

In the strong coupling regime $\{|W_{12}| \gg |V_{03}|\}$ in Eq. (6) the equilibrium position of one rotor with respect to the other is well defined and the two dynamics are separable. Then, the Hamiltonian is rewritten as:

$$H_{2ia} = H_{2i}(\theta_i) + H_{2a}(\theta_a) \quad (7)$$

with

$$\begin{aligned} H_{2i}(\theta_i) &= -\frac{B}{2} \frac{\partial^2}{\partial \theta_i^2} + \frac{V_{3i}}{2} \cos 3\theta_i \\ H_{2a}(\theta_a) &= -\frac{B}{2} \frac{\partial^2}{\partial \theta_a^2} + \frac{V_{3a}}{2} \cos 3\theta_a + \frac{W_{12a}}{2} \cos 6\theta_a \end{aligned} \quad (8)$$

For in-phase rotation the coupling term vanishes and the dynamics is that of a single rotor with moment of inertia $2I_r$ experiencing a threefold potential. If the coupling potential is strongly attractive the pair is in the eclipsed conformation and the effective potential is $V_{3i} \approx 2V_{03}$. Alternatively, if the staggered configuration is favored by a repulsive coupling term,

the effective sixfold potential should be very weak and give rise to nearly free rotation. In that case, V_{03} in Eq. (6) cannot be determined experimentally. (This is the price for the separation of the dynamics but this is not really a penalty since free rotation is always due to a delicate balance between many contributions). For anti-phase rotation, the effective potential comprises a contribution from both V_{3a} and W_{12} .

An important consequence of the symmetry adapted coordinate is that the rotational constant is divided by a factor 2 compared to the single rotor. The maximum frequency for free rotation is now in the range 0.325 – 0.350meV for a pair of CH₃ and 0.162 – 0.175meV for a pair of CD₃. Therefore, the transitions observed around 0.270meV may correspond to pairs rotating almost freely, in accordance with measurements of the spin-lattice relaxation.²⁹

The energy level scheme for tunnelling presented in Figure 7B is composed of one tunnelling state for in-phase rotation in a three-fold potential ($|0_{E\pm}\rangle_i$) and three states for anti-phase rotation in a six-fold potential ($|0_{E\pm}\rangle_a$, $|1_{E\pm}\rangle_a$ and $|1_A\rangle_a$). There are four fundamental transitions ($|0_A\rangle \rightarrow |0_{E\pm}\rangle_i$, $|0_A\rangle \rightarrow |0_{E\pm}\rangle_a$, $|0_A\rangle \rightarrow |1_{E\pm}\rangle_a$ and $|0_A\rangle \rightarrow |1_A\rangle_a$) and two "hot" transitions ($|0_{E\pm}\rangle_a \rightarrow |1_{E\pm}\rangle_a$ and $|0_{E\pm}\rangle_a \rightarrow |1_A\rangle_a$). Even at 1.5 K, the $|0_{E\pm}\rangle_a$ level at ≈ 0.030 meV is largely populated (80%) and temperature effects on the band intensity is marginal. However, if hot transitions were not resolved from their parent bands, the attribution of the four transitions previously distinguished in the spectrum^{7,6} should be straightforward.

3.6. Isotope mixtures

A more focussed view of the rotational dynamics was tentatively sought for with mixtures of CH₃ and CD₃ derivatives.⁶ The physical and chemical differences for the two analogues are negligible compared to intermolecular interaction in the crystal, and mixtures are statistical distributions of pairs. If x and $(1 - x)$ are the relative concentrations of CD₃ and CH₃, respectively, then, the relative concentrations of pairs CH₃–CH₃, CH₃–CD₃ and CD₃–CD₃ are $(1 - x)^2$, $2x(1 - x)$ and x^2 , respectively.

According to the energy level scheme in Figure 7A, the totally decoupled mixed pairs have four tunnelling levels: $|A_H A_D\rangle$, $|A_H E_D\rangle$, $|E_H A_D\rangle$ and $|E_H E_D\rangle$. Since $|E_H\rangle$ and $|E_D\rangle$ states are quite separate the splitting arising from the relative rotation of the two tops ($|E_H^\pm E_D^\pm\rangle$ and $|E_H^\pm E_D^\mp\rangle$) can be ignored. This decoupling is the normal consequence of the removal of the indistinguishability for mixed pairs. Therefore, the spectrum is composed of degenerate transitions $|A_H\rangle \rightarrow |E_H\rangle$ and $|A_D\rangle \rightarrow |E_D\rangle$ for decoupled CH₃ and CD₃ tops, respectively. If there were no change of the effective

potential upon isotope substitution, the frequency for a decoupled rotor should be at the barycenter of the spectral profile for the coupled pair.

The tunnelling spectra of mixtures containing small concentrations of CH_3 (from 5 to 20%) in CD_3 environment were decomposed into a main peak at 0.130meV and a weak shoulder at 0.180meV attributed to $\text{CH}_3\text{--CD}_3$ and $\text{CH}_3\text{--CH}_3$ pairs, respectively.⁶ For an increasing concentration of CH_3 rotors, the intensity at 0.130meV decreases, that at 0.180meV increases to a maximum value for a concentration of 66% and then decreases whilst new features centered at 0.250meV appear. Therefore, there are at least 3 bands instead of the 2 anticipated with the model. The extra band was attributed to $\text{CH}_3\text{--CH}_3$ pairs surrounded by deuterated rotors. The effective potential barrier is increased and the band at 0.250meV is shifted downward to 0.180meV. However, each pair has four nearest neighbors methyl groups to which should correspond four different environments and effective potentials in isotope mixtures. If the different environments are not resolved, a smooth frequency shift should be observed, rather than a change of relative intensities for well separate transitions.

The interpretation of the spectra is hampered by the different crystal structures for the CH_3 and CD_3 derivatives. The phase transitions may take place at various temperatures depending on the isotope concentration and it is difficult to distinguish dynamical and structural effects. In this context, isotope mixtures of CH_3 and CH_2D derivatives are more appropriate. There is no phase transition (this point deserves further confirmation) and the perturbation of the effective potential, if any, is minimized. Moreover, a great advantage compared to CD_3 is that CH_2D rotors have significant scattering cross section. Therefore, tunnelling arising from each pair $\text{CH}_3\text{--CH}_3$, $\text{CH}_3\text{--CH}_2\text{D}$ and $\text{CH}_2\text{D--CH}_2\text{D}$ can be observed. However, owing to the different pair potentials for $\text{H}\dots\text{H}$, $\text{H}\dots\text{D}$ and $\text{D}\dots\text{D}$ atoms,¹³ anti-phase tunnelling is cancelled for $\text{CH}_2\text{D--CH}_2\text{D}$ pairs.

The spectra presented in Figure 8 provide more detailed information than those previously reported.⁶ They were decomposed into rather narrow components with relative intensities depending on the isotope concentration. The relative frequency shift for each component is less than 10%, which suggests quite moderate changes of the effective potential. For the sake of continuity, the spectra of the mixtures containing 80% and 100% of CH_3 were decomposed into 4 components between 0.150 and 0.300meV, instead of three reported previously.^{7,8,6} Therefore, the symmetry adapted coordinates in Eqs (7) and (8) and the energy level scheme in Figure 7 are the most realistic.

At a low concentration in CH_3 (20%) the most intense band at 0.166meV

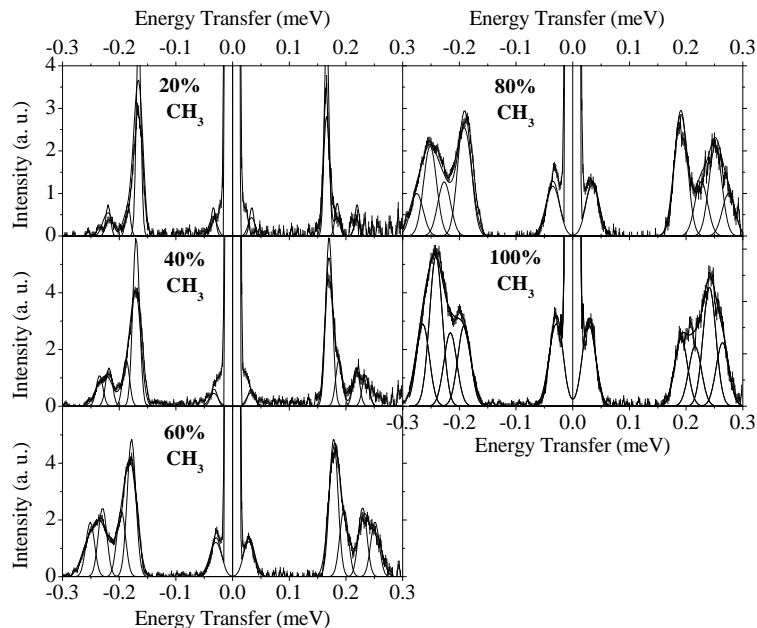


Figure 8. INS spectra and tentative band decomposition of isotope mixtures of $\text{CH}_3\text{COOLi}, 2\text{H}_2\text{O}$ and $\text{CH}_2\text{DCOOLi}, 2\text{H}_2\text{O}$ at 1.7 K, after ref. 15.

and the weaker band at 0.185 meV can be attributed to in-phase rotation of $\text{CH}_2\text{D}-\text{CH}_2\text{D}$ ($B = 0.246\text{meV}$) and $\text{CH}_3-\text{CH}_2\text{D}$ ($B = 0.281\text{meV}$), respectively. The weak transition at 0.220 meV is tentatively assigned to anti-phase tunnelling of $\text{CH}_3-\text{CH}_2\text{D}$.

For increasing concentration in CH_3 the band intensity around 0.170 meV decreases whilst the frequency shifts smoothly upwards to 0.191 meV for 100% of CH_3 rotors. This behavior suggests unresolved transitions due to $\text{CH}_2\text{D}-\text{CH}_2\text{D}$ and CH_3-CH_3 pairs, respectively. We extrapolate the frequency for in-phase tunnelling of $\text{CH}_2\text{D}-\text{CH}_2\text{D}$ pairs to be 0.164 meV. The band intensity at $\approx 0.030\text{meV}$ due to out-of-phase rotation of symmetric CH_3-CH_3 pairs and the intensities of the three bands at high frequency increase simultaneously with the concentration in CH_3 .

With the unambiguous assignment of the in-phase tunnelling for CH_3-CD_3 (0.130 meV) and $\text{CH}_2\text{D}-\text{CH}_2\text{D}$ (0.164 meV), we assign the transition at 0.241 meV in $\text{Li}ac-h_7$ to in-phase tunnelling of CH_3-CH_3 entities. The average of the estimated potential values for pairs containing H atoms is $V_{3i} = (1.82 \pm 0.15)\text{meV}$. The rather modest dispersion of $\approx 10\%$ may arise from experimental errors, band shape analysis and variations of the

effective potential with the mass.

For anti-phase rotation we have virtually no information for the deuterated species. For $\text{CH}_3\text{--CH}_3$ pairs, we assign the doublet at 0.191 and 0.216meV to $|0_{E\pm}\rangle_a \rightarrow |1_{E\pm}\rangle_a$ and $|0_A\rangle \rightarrow |1_{E\pm}\rangle_a$, respectively. The splitting of 0.025meV compares to the $|0_A\rangle \rightarrow |0_{E\pm}\rangle_a$ transition observed at 0.029meV. Similarly, we assign the component at 0.264meV to $|0_A\rangle \rightarrow |1_A\rangle_a$ and we suppose that the companion transition $|0_{E\pm}\rangle_a \rightarrow |1_A\rangle_a$ anticipated at 0.235meV is a part of the main band at 0.241meV. Here we suppose that all transitions have virtually the same intensity. The best fit is obtained with the effective potential terms in Eq. (8) $V_{3a} = 0.19$ and $W_{12a} = 31.64$, in meV units. As anticipated for staggered methyl groups, the on-site potential is almost perfectly cancelled. The condition $W_{12a} \gg V_{3a}$ is for well separate in-phase and anti-phase dynamics is largely satisfied.

3.7. Coupling between pairs and phase transition mechanism

The phase transition is related to long-range ordering of the methyl groups in the honeycomb-like arrangement of acetate entities in the (a,b) plane (see Figure 5). Owing to the great stability of the positions of heavy atoms that remain virtually unchanged through the phase transition, the local potential arising from the mean crystal field is not changed. Therefore, the key parameter for the effective coupling between adjacent pairs of rotors is the angular mean-amplitude depending on mass and temperature $\bar{\theta}(T) = \langle \theta^2(T) \rangle^{1/2}$ with:

$$\langle \theta^2(T) \rangle = \int_{-\pi/3}^{\pi/3} d\theta P(\theta, T) \theta^2. \quad (9)$$

For anti-phase dynamics coupling between adjacent pairs is negligible compared to the high sixfold potential barrier. For in-phase rotation, the rather weak effective on-site potential can be attributed to interaction between pairs. The Hamiltonian including coupling with the four nearest-neighbors of a pair (see Figure 9) can be written as:

$$H_{ci} = -\frac{B}{2} \frac{\partial^2}{\partial \theta_i^2} + \frac{V_{03i}}{2} (1 - \cos 3\theta_i) + \sum_{n=1}^4 \frac{V_{ci}}{2} [1 - \cos 3(\theta_{in} - \theta_i)]. \quad (10)$$

In the weak-coupling (between pairs) regime, there is no correlation between the angular coordinate of the pair (θ_i) and those of the neighbors (θ_{in}) . The

effective potential can be thus expanded as:

$$\begin{aligned} \frac{V_{3i}}{2} (1 - \cos 3\theta_i) &= \frac{V_{03i}}{2} (1 - \cos 3\theta_i) \\ &+ \sum_{n=1}^4 \frac{V_{ci}}{2} (1 - \cos 3\theta_i \cos 3\theta_{in} - \sin \theta_i \sin \theta_{in}). \end{aligned} \quad (11)$$

Averaging over the distribution of phase differences gives then the effective potential:

$$V_{3i}^{eff} \approx V_{03i} + 4V_{ci} \cos [3\bar{\theta}(T)], \quad (12)$$

With the potential functions determined at low temperature for in-phase rotation, $\bar{\theta}_{iH} \approx 21^\circ$ for CH₃ pairs and $\bar{\theta}_{iD} \approx 11^\circ$ for CD₃ analogues. Then, if the increase of the effective potential barrier from ≈ 1.9 to ≈ 4.5 meV upon methyl deuteration is due to the change of $\bar{\theta}(T)$ we obtain $4V_{ci} \approx 9.2$ meV and $V_{03i} \approx -3.7$ meV. The opposite signs mean that the methyl orientation favored by the on-site potential is opposite to the orientation favored by interaction with next nearest neighbors. The effective potential in Eq. (12) vanishes for $\bar{\theta}_0 \approx 22^\circ$. This is the key parameter to account for the phase transition upon deuteration.

for CH₃ pairs, $V_{3i}^{eff} \approx 1.8$ meV. There is no long-range correlation for methyl orientation at any temperature. The density probability derived from the rotational wave functions is markedly localized. Therefore, the delocalized angular density distribution observed with diffraction means that methyl group are statistically distributed among several orientations. In this case, dynamical and statistical probability densities can be distinguished. This was largely overlooked in previous calculations with quantum chemistry methods.¹⁹

For CD₃, the long-range interaction is dominant at 14K and the orientation of the CD₃ groups along the *a* axis is imposed by the interaction between methyl groups. In the absence of this methyl-methyl interaction along *a*, the orientation of the pairs would be rotated by $\pi/3$. As the temperature is increased, the rotational levels at ≈ 2 meV are populated, the mean angular amplitude increases and the long-range ordering decreases. The phase transition takes place when the thermal bath energy is similar to ≈ 2 meV or ≈ 22 K. This value compares favorably to the temperature of 17.5 K for the phase transition.

4. Quantum rotational dynamics for infinite chains of coupled rotors

In the 4MP crystal the rotation of methyl-groups is nearly free^{30,31,32} but the dynamics are quite different from those in lithiumacetate dihydrate and

this is a consequence of the different crystal structures for the two systems (compare Figures 9 and 5).

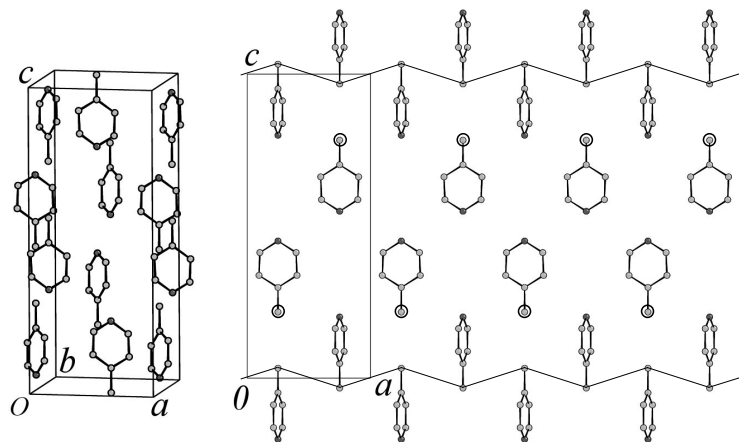


Figure 9. Schematic view of the structure of the 4-methylpyridine crystal at 10 K, after ref. 33. Left: view of the unit cell. Right: projection onto the (a, c) plane showing the infinite chains parallel to a (along the zigzag line) or parallel to b (circles). For the sake of clarity, all H-atoms are hidden.

In the tetragonal structure ($I4_1/a$) all molecules are equivalent.³⁴ The C–C rotational axes are parallel to the c axis. The C_2 site symmetry impose disordering of the methyl groups and even at 10 K the angular probability density is virtually isotropic.³³ The structure remains unchanged until the first order phase transition at 254 K, close to the melting point at 276.8K. There is no further phase transition for the deuterated crystal.³⁵

The shortest intermolecular distances of ≈ 3.46 Å between face-to-face methyl groups parallel to the c axis and the next shortest methyl-methyl distances of ≈ 4.0 Å perpendicular to the c axis, are quite similar to distances in lithiumacetate dihydrate (≈ 3.3 and 3.4 Å, respectively, see section 3 and Figure 5). However, in contrast to the honey-comb like arrangement, the equidistant methyl groups in 4-methylpyridine form two equivalent sets of orthogonal infinite chains parallel to the a and b crystal axes. The zigzag lines in Figure 9 correspond to chains parallel to a and circles represent intersections with the (a, c) plane of chains parallel to b . There is only one close-contact pair in common for nearest orthogonal chains.

Within the tetragonal symmetry, to any particular orientation of a

methyl group corresponds 4 indistinguishable orientations obtained by symmetry with respect to the molecular plane and by $\pm\pi/2$ rotations. The twelve equivalent proton sites for a pair give a quasi-isotropic ring for the density distribution. Each methyl group experiences a virtually isotropic mean-field corresponding to the pair potential averaged over all orientations. The effective intra-pair potential is a constant and there is no coupling between collective excitations along a or b . Collective rotational dynamics occur exclusively in 1D.

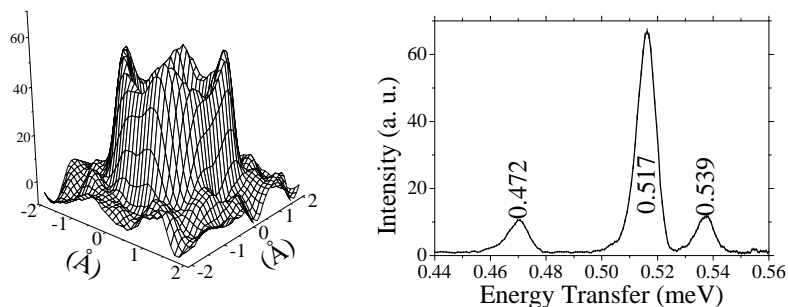


Figure 10. Left: probability density distribution of protons in the rotational plane of 4-methylpyridine at 10 K, after ref. 33. Right: the INS tunnelling spectrum of 4-methylpyridine at 0.5 K after ref. 13

These conclusions emphasize that a superficial examination of the intra-pair distances can be misleading. For example, Ohms and co-workers³⁴ concluded that the crystal structure implies strong correlation between the mutual orientations of adjacent methyl-groups which would have to be twisted by 60° with respect to each other and perform combined hindered rotations. Similarly, it is dangerous to utilize calculations of the effective potential, even with advanced quantum chemistry methods, for molecular-dynamics simulations without caution. Quantum chemistry gives logically a large coupling potential term for the close-contact pairs if the local symmetry is relaxed. Then, molecular dynamics simulation within the framework of classical mechanics give a false view of the methyl rotation.³⁶

The tunnelling spectrum of 4-methylpyridine is totally different from that of lithium acetate. Early INS measurements with rather modest resolution have revealed a tunnelling transition at $\approx 0.5\text{meV}$ and this was regarded as a manifestation of nearly free rotation.³⁰ This was the first observation of rotational tunnelling with INS and this remains the highest tunnelling frequency ever reported for a methyl group.

Further INS experiments with better resolution have revealed a complex spectrum composed of an intense band at 0.517(4)meV and weaker bands at 0.472(4)meV and 0.539(4)meV (see Figure 10).¹² The splitting arises from dynamical correlation and a model based on coupled pairs of rotors, with some similarity with lithiumacetate dihydrate, was first proposed.³⁷ However, this is unlikely regarding the crystal structure.

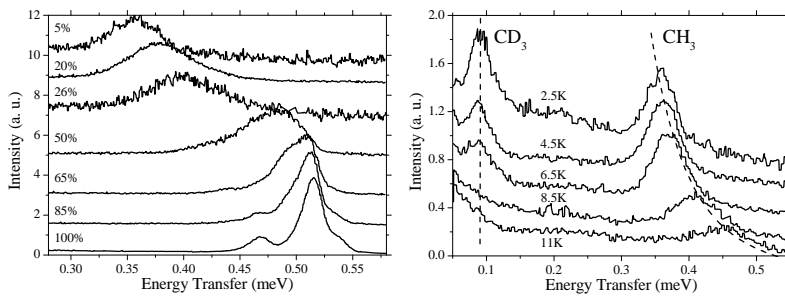


Figure 11. Tunnelling spectra of isotopic mixtures of hydrogenated and deuterated molecules, after ref. 12. Left: various concentrations of 4MP- h_7 at 2.5 K. Right: temperature effect for the mixture containing 5% of 4MP- h_7 and 95% of 4MP- d_7 . Dash lines are guides for eyes.

The INS spectra of isotopic mixtures containing hydrogenated and deuterated molecules (4MP- h_7 and 4MP- d_7 , respectively) show dramatic frequency shifts (up to $\Delta\nu/\nu \approx 30\%$), depending on concentration and temperature (see Figure 11)¹² which cannot be explained with any coupled pair model.³⁸ These experiments establish the collective nature of the methyl group dynamics and this was represented with the quantum sine-Gordon theory.¹²

4.1. The quantum sine-Gordon

This section is a summary of the relevant equations. More details were presented in refs 12,13,16. The Hamiltonian for an infinite chain of coupled rotors can be written as:

$$H = \sum_j -\frac{\hbar^2}{2I_r} \frac{\partial^2}{\partial \theta_j^2} + \frac{V_0}{2} (1 - \cos 3i\theta_j) + \frac{V_c}{2} [1 - \cos 3i(\theta_{j+1} - \theta_j)], \quad (13)$$

where θ_j is the angular coordinate of the j th rotor in the one-dimensional chain with parameter L . V_0 is the on-site potential which does not depend on lattice position, and V_c is the coupling ("strain" energy) between neighboring rotors. The index $i = 1, 2 \dots$ determines the potential periodicity

compatible with the C_{3v} symmetry of the methyl-groups. In the strong coupling (or displacive) limit, when $\theta_{j+1} - \theta_j$ is sufficiently small, Eq. (13) is equivalent to the sine-Gordon equation:

$$H \approx \sum_j -\frac{\hbar^2}{2I_r} \frac{\partial^2}{\partial \theta_j^2} + \frac{V_0}{2} (1 - \cos 3i\theta_j) + \frac{(3i)^2 V_c}{4} (\theta_{j+1} - \theta_j)^2. \quad (14)$$

If variations of θ from site to site are small, then the site index can be replaced by a continuous position variable x (see Figure 12). Kinks, rotons (phonons) and breathers are the elementary excitations.^{39,40,41,42,43,44,45,46,47,48,49,50,51} Since the kink density vanishes at low temperature and phonons are beyond the spectral range under investigation, these excitations can be ignored.

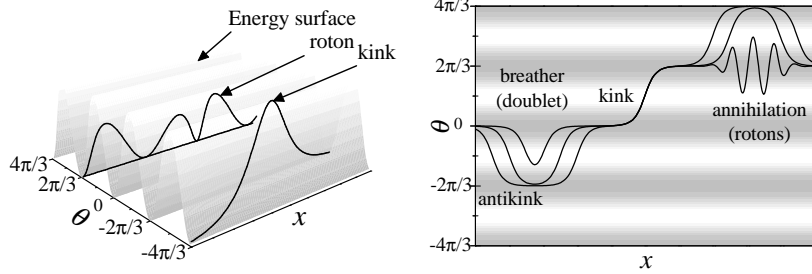


Figure 12. Artistic view of the sine-Gordon excitations.

The breather or doublet is a well-defined elementary nonlinear excitation with long life-time and as such behaves very much like a particle. In the classical regime, the waveform is:

$$\varphi_B^v(x, t) = 4 \text{Arct} \left[\frac{\sqrt{\frac{\omega_0^2}{\omega_B^2} - 1} \sin \frac{\omega_B (t - vx/c_0^2)}{\sqrt{1 - v^2/c_0^2}}}{\cosh \frac{(x - vt) \sqrt{1 - \omega_B^2/\omega_0^2}}{d \sqrt{1 - v^2/c_0^2}}} \right] \quad \text{with} \quad \begin{cases} \omega_0^2 = \frac{V_0(3i)^2}{2I_r}; \\ c_0^2 = \frac{V_c L^2 (3i)^2}{2I_r} = \omega_c^2 L^2; \\ d = \frac{c_0}{\omega_0}. \end{cases} \quad (15)$$

The breather envelope travelling at velocity v is oscillating harmonically at frequency ω_B which may vary continuously from 0 to ω_0 . Breathers can be viewed as kink-antikink bound states (Figure 12).

In the quantum regime^{40,41} the classical breather yields a discrete spectrum of mass at rest ${}^qM_{B,l}^0$ depending on the quantum number l :

$${}^qM_{B,l}^0 = 2 {}^qM_{K\pm}^0 \sin \frac{l(3i)^2}{16 \left[1 - \frac{(3i)^2}{8\pi}\right]} \text{ with } l = 1, 2, \dots < \frac{8\pi}{(3i)^2} - 1 \quad ; \quad (16)$$

${}^qM_{K\pm}^0$ is the renormalized mass at rest of the classical kink:

$${}^qM_{K\pm}^0 = \frac{8I_r}{(3iL)^2} \left[1 - \frac{(3i)^2}{8\pi}\right] \text{ and } 3i < \sqrt{8\pi}. \quad (17)$$

In the case of methyl-groups, the breather-mode of the quantum sine-Gordon theory exists only for the threefold potential. Then, there is only one mass state ($l=1$) and this is the fundamental state. For energy transfer below the dissociation threshold corresponding to the creation of a kink-antikink pair, only kinetic energy can be transferred to the breather. This defines the dispersion law as:

$${}^qE_{B,l}(p_B) = \sqrt{{}^qE_{B,l}^{02} + p_B^2 c_0^2}; \quad (18)$$

where ${}^qE_{B,l}^0 = {}^qM_{B,l,0} c_0^2$ is the energy at rest of the breather mode and p_B is the kinetic momentum. Because the Hamiltonian in Eqs (13) and (14) possess translational invariance, the ground state can be represented with breathers at rest totally delocalized along the chain. The de Broglie wave length associated to the pseudo-particle is $\lambda = \infty$. The breather can propagate along the chains if, and only if, the de Broglie wavelength is an integral fraction of the lattice parameter:¹³

$$\lambda = \frac{h}{p_B} = \frac{L}{n}, \quad n = 0, \pm 1, \pm 2, \dots \quad (19)$$

Then, the kinetic energy spectrum is:

$${}^qE_{B,l,n} = \sqrt{{}^qE_{B,l,0}^2 + n^2 \hbar^2 \omega_c^2}. \quad (20)$$

Eq. (20) is in accord with the INS^{12,13,16}, infrared and Raman^{10,11} spectra of the 4-methylpyridine crystal. The band at 0.517meV in pure 4MP- h_7 (Figure 10) corresponds to the $0 \rightarrow 1$ transition between the travelling-states.

In Eq. (14) the periodical nature of the methyl-group rotation was discarded by the expansion of the coupling term. Consequently, collective tunnelling is not included in the sine-Gordon Hamiltonian. In the full Hamiltonian, Eq. (13), methyl tunnelling can be regarded as a one-dimensional band-structure problem. The dispersion law can be computed

numerically. The tunnel splitting in the ground state varies continuously between two extremes located at the zone center, where the methyl groups are tunnelling in-phase, and at the zone boundary, where tunnelling occurs out-of-phase:

$$\begin{aligned} H_{ip} &= -\frac{\hbar^2}{2I_r} \frac{\partial^2}{\partial \theta_j^2} + \frac{V_0}{2} (1 - \cos 3i\theta) \\ H_{op} &= -\frac{\hbar^2}{2I_r} \frac{\partial^2}{\partial \theta_j^2} + \frac{V_0}{2} (1 - \cos 3i\theta) + \frac{V_c}{2} (1 - \cos 6i\theta). \end{aligned} \quad (21)$$

These extremes correspond to the maxima of the density-of-states observed with the INS technique. Consequently, the bands at 0.537 and 0.470meV in pure 4MP- h_7 (see Figure 10) were attributed to in-phase and out-of-phase tunnelling transitions of the chain, respectively.

In the sine-Gordon theory three transitions (namely, two tunnelling and one breather-travelling mode) are determined with two parameters: V_0 and V_c . The potential barriers in Eq. (21) were first determined to fit the observed tunnelling transitions at 0.539 (in-phase) and 0.472meV (out-of-phase). Then, the calculated energy at rest of the breather mode and the first travelling state correspond to observation with better than 10% accuracy. This is remarkable since the sine-Gordon equation is an approximation of the Hamiltonian for the chain, which is already an approximation of the real system under consideration. The full width at half maximum of the breather waveform is about $5L$ (see below Figure 14) and numerical calculations confirm that the pinning potential in the discrete lattice is virtually zero. It is thus confirmed that the continuous limit approximation is relevant.

4.2. Breather dynamics in isotopic mixtures

In isotopic mixtures 4MP- h_7 and 4MP- d_7 molecules are distributed randomly among the crystal sites. They form clusters of various sizes, s_h and s_d , respectively. The rotational constant of the deuterated methyl-group being divided by a factor of 2 with respect to the hydrogenated analogue, the travelling-states are quite different. The translational invariance is broken and bound-states are observed for breathers. The frequency shifts observed at a very low temperature can be explained with reflective walls at cluster boundary.¹² The lowest travelling state in a cluster is determined by the size (sL) of the box, such as: $\lambda = sL$. Transitions between travelling states are then:

$$\begin{aligned} \nu_{sn} &= \sqrt{qE_{B,l,0}^2 + n^2\hbar^2\omega_c^2} - \sqrt{qE_{B,l,0}^2 + \hbar^2\frac{\omega_c^2}{s^2}} \quad ; \\ n &= \pm 1, \pm 2, \dots \quad ; \quad s = 1, 2, \dots \end{aligned} \quad (22)$$

As the cluster size decreases, the energy of the ground state increases with respect to that of the infinite chain and the frequency of the transition decreases. This equation accounts for the frequency shift of the main band from 0.517 to 0.360meV (Figure 10). This view provides also a straightforward mechanism to account for the frequency shift with temperature (see Figure 11). As the temperature increases, a continuum of breather-rotor states is populated and can bridge the gap between adjacent clusters. Then, the trapped breather becomes progressively free and the travelling transition shifts continuously from 0.360 backwards to 0.500meV.

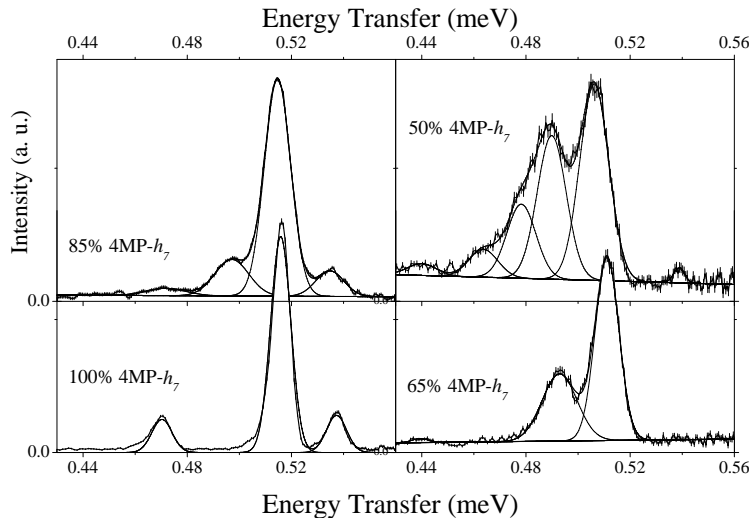


Figure 13. Inelastic neutron scattering spectra of isotopic mixtures of $4\text{MP}-h_7$ and $4\text{MP}-d_7$. The temperature was 0.5 K for 100% $4\text{MP}-h_7$ and 1.8 K for the mixtures, after ref. 16.

For modest concentrations of deuterated molecules the INS spectra obtained with better resolution reveal a more complex behavior (see Figure 13). The previously unresolved broad bands in Figure 10 are now resolved into several components. The breather band at 0.517meV in pure $4\text{MP}-h_7$ shifts downwards slightly as the concentration of deuterated molecules increases ($\approx 0.506\text{meV}$ for 50% of $4\text{MP}-d_7$). The weak tunnelling bands disappear rapidly whilst new bands appear with increasing intensities with the concentration of deuterated species. These spectra are well explained with the quantum sine-Gordon theory.

At a low concentration, the deuterated molecules are largely isolated. For a single chain the mean size of hydrogenated clusters is then proportional to the inverse of the concentration of deuterated molecules: $\bar{s}_h \approx 2/c_d$. However, the pairs of indistinguishable molecules along the c axis give rise to a twofold degeneracy. Consequently, the mean cluster size for a chain is $\bar{s}_h \approx 4/c_d$. Expansion of Eq. (21) for $c_d \ll 1$ gives the mean frequency for the travelling transition of the breather:

$$\bar{\nu}_{01} \approx \frac{\hbar^2 \omega_c^2}{2^q E_{B,l,0}^2} \left(1 - \frac{c_d^2}{16} \right) \quad (23)$$

This equation is rather close to the observation (Figure 14 Left). It may

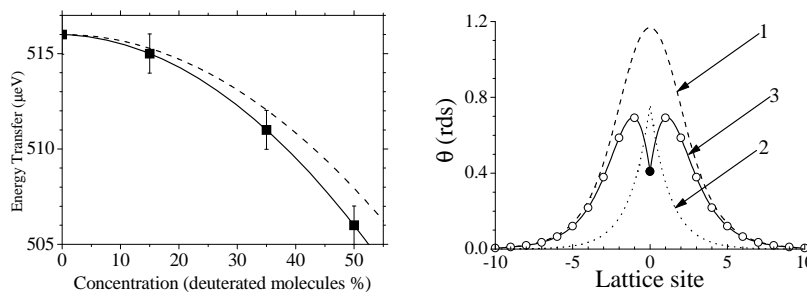


Figure 14. Left: variation of the main band frequency with the concentration of deuterated molecules. Data points: solid squares. Best fit: solid line with $\nu = 516 \left(1 - 0.074c_d^2 \right)$. Dash line: theory according to Eq. (23). Right: wave form of the breather (1, dash), of the plasma wave (2, short dash) and of the breather (3, solid line) interacting with a single deuterated impurity (solid circle) surrounded by hydrogenated molecules (circles). after ref. 16.

be concluded that the observed frequency shift is essentially due to the collective nature of the dynamics. The twofold degeneracy confirms that the chain dynamics are essentially 1D in nature, with no significant contribution of the methyl-methyl interaction within the close-contact pairs. Dynamics along the a or b axis are totally uncorrelated and degenerate.

The band at ≈ 0.490 meV in isotopic mixtures (see Figure 13) cannot be rationalized with the cluster size statistics presented above. The frequency corresponds roughly to that anticipated for clusters with s_h between 4 and 5. However, the intensity is virtually proportional to the amount of deuterated molecules whereas the amount of small clusters should be proportional to the square of the concentration. Therefore, this band was attributed to breathers trapped by isolated deuterated molecules.

The Hamiltonian representing an infinite chain of hydrogenated molecules containing a single deuterated molecule at the site $j = 0$ can be written as:¹⁶

$$H = \sum_j -\frac{\hbar^2}{2I_r} \frac{\partial^2}{\partial \theta_j^2} + \frac{V_0}{2} (1 - \cos 3i\theta_j) + \frac{V_c}{2} [1 - \cos 3i(\theta_{j+1} - \theta_j)] + \frac{\hbar^2}{4I_r} \frac{\partial^2}{\partial \theta_0^2} \quad (24)$$

The impurity is equivalent to a driving force at frequency $\omega_B/2\pi$, below the lowest phonon frequency at $\omega_0/2\pi$. A solution of the approximate Hamiltonian linearized with respect to the potential minimum is the standing plasma-wave centered at site $j = 0$ whose amplitude decreases exponentially on both sides (see Figure 14).⁵¹ The waveform of a breather centered at x_B interacting with the impurity is :

$$\Theta(x, t) = \Phi_B(x - x_B, t) - \Phi_B(-x_B, t) \frac{\exp\left(-\sqrt{1 - \omega_B^2/\omega_0^2} |x|\right)}{2\sqrt{1 - \omega_B^2/\omega_0^2}} \quad (25)$$

The waveform is represented for $x_B = 0$ in Figure 14. The breather is attracted by the impurity and the effective potential averaged over the fast internal oscillation is:⁵¹

$$U_{eff}(x) = -4F \cot \mu \cosh(x \sin \mu) [1 + \cot^2 \mu \cosh^2(x \sin \mu)]^{-3/2} \quad (26)$$

with $\mu = \frac{(3i)^2}{16[1 - (3i)^2/8\pi]}$. The shape of the effective potential resembles the form of the breather-wave. The width at half minimum ($\Delta U_{eff} \approx 4-5$ lattice sites) gives the amplitude of the breather center-of-mass oscillations around the impurity. Thus, the travelling transition is anticipated between 0.485 and 0.500meV,¹² in accord with the observation. The band at 0.490meV is thus an experimental confirmation that the width of the breather wave is $\approx 4-5$ lattice sites. The effective potential tends to zero exponentially as x goes to infinity and impurities separated by more than ≈ 5 lattice sites are virtually isolated.

According to the energy at half minimum of the effective potential (≈ 0.5 meV/6 K), the breather is trapped only at a low temperature.¹² The frequency of the travelling state increases with temperature, up to the frequency of the unperturbed breather.

4.3. Discussion

To the best of our knowledge the 4-methylpyridine crystal is a unique example of sine-Gordon dynamics in the quantum regime. The quantum sine-Gordon theory for infinite chains of coupled rotors accounts for a

long list of experiments (four transitions –INS and Raman–, isotope mixtures, temperature effects, partial deuteration...) with only two parameters V_0 and V_c . Experiments have confirmed theoretical predictions for the quantization of the breather internal energy^{40,41} or interaction with local impurities.⁵¹ Some observations are directly related to the width of the breather waveform and can be regarded as direct evidence of the existence of this soliton. Conversely, experiments emphasize the dimensionless-pseudoparticle/planar-wave character of the breather mode and quantization of the travelling mode is a natural consequence of the Bragg rule. The crystal lattice “tolerates” the breather mode, although an exact solution only in the continuous limit, but, owing to discreteness, it “restricts” the travelling velocity and kinetic energy to a series of discrete extended states, *via* diffraction. This has been overlooked in theoretical works.⁵⁴ Measurements currently in progress confirm the anisotropy anticipated for particles travelling along chains parallel to the a and b crystal axes. The discrete spectrum in momentum space is markedly different from a phonon band structure and the main consequence of nonlinearity turns out to be localization in momentum rather than in position.

Alternative theoretical approaches proposed during the last decade (all of them have not been published yet) were not able to fit the data with reasonable accuracy and/or with such a limited number of parameters.^{36,37,38,52,53,54,55}

Voll³⁸ has extended the coupled pair of Clough⁷ to a quantum mechanical treatment of loops containing many coupled rotors, with the motivation of extrapolating to the infinite chain limit. He concluded that the tunnelling spectra should be hardly distinguishable from that of the single rotor but the interpretation in terms of single rotor potential would be erroneous. This conclusion is quite pertinent for 4-methylpyridine. However, calculations are so cumbersome that they were limited to the maximum number of four coupled rotors in a loop. Further developments are necessary in order to achieve reasonable modelling of the 4-methylpyridine crystal.

Neumann³⁶ has calculated potential terms in the 4-methylpyridine crystal with quantum chemistry methods. He has considered coupling between four nearest-neighbor methyl-groups. In addition, he introduced precession-rotation, as Schiebel and co-workers¹⁹ did for lithiumacetate, which amounts to consider coupling with phonons. Finally, the complex potential function for methyl rotation depends on a very large number of parameters (approximately 8, but this was not clearly stated) in addition to rescaling the rotational constant, as a consequence of precession. With so many parameters the model is not unique, and the contact with real physics

is questionable. The calculated spectrum of 4MP- h_7 looks very nice but the continuous frequency shift in isotope mixtures is not accounted for.

The ambiguity of the term “breather” in nonlinear sciences has been a source of more or less artificial/semantical controversies. Breathers are often regarded as manifestations of intrinsic energy localization in nonlinear lattices upon energy transfer to sufficiently high excited states.^{56,54} In the classical regime, sine-Gordon breathers can be regarded as nonlinear excitations with a continuum of internal amplitude to which energy can be transferred. However, the internal frequencies of the breathers are always markedly below the roton density-of-states. In the quantum regime, the sine-Gordon breather is totally different and may appear rather paradoxical, as usually the case in the quantal world. The continuum of internal energy turns into a discrete spectrum depending on a specific quantum number. Moreover, in the particular case of threefold periodicity for the on-site potential there is only one mass state and this is a part of the ground state. This breather cannot be annihilated or created and it cannot be regarded any more as an “excitation”. Although this property of the quantum sine-Gordon dynamics was emphasized by Dashen and co-workers,⁴⁰ this view has been contended by MacKay⁵⁵ who claimed that this is misunderstanding theoretical works. In order to avoid any further polemical discussions, it is necessary to reconsider the Lagrangian as formally written by Dashen and co-workers:⁴⁰

$$\mathcal{L} = \frac{1}{2} (\partial_\mu \phi)^2 + \frac{m^4}{\lambda} \left[\cos \left(\frac{\sqrt{\lambda}}{m} \phi \right) - 1 \right]. \quad (27)$$

The mass states for the breather are $M_n = (16m/\gamma') \sin(n\gamma'/16)$ with $\gamma' = (\lambda/m^2) [1 - \lambda/(8\pi m^2)]^{-1}$. Coleman⁴² has emphasized the meaning of $\sqrt{\lambda}/m$ in the quantization of the sine-Gordon Hamiltonian. In classical mechanics, changing this factor amounts to multiplying the Hamiltonian by a constant and this has no effect other than redefining the energy-scale. In the quantum regime, the energy scale is determined by $\hbar\lambda/m^2$ and a change of $\sqrt{\lambda}/m$ is equivalent to rescaling the Planck’s constant h . Therefore, the periodicity of the on-site potential for methyl rotors imposes $\sqrt{\lambda}/m = 3$. This is a non-adjustable value and all parameters in Eq. (14) were determined accordingly.¹² (Much the same, the choice of symmetry adapted angular coordinates for coupled rotors, in section 3.5, must be compatible with the potential periodicity.) The alternative value of 1.46 proposed by MacKay is obviously irrelevant for methyl rotation. This author also questioned the quantization of the travelling mode, arguing that this does not apply to electrons in metals. It is quite difficult to follow this line

of reasoning. Is it possible to ignore that electrons, and other particles, can be diffracted by crystal lattices according to the Bragg law? Even more surprising, the same author suggested that the disappearance of the breather transition on a time-scale of ≈ 70 hours¹⁴ supports the decay of the breather mode itself at low temperature. However, this is a dramatic confusion between up and down scattering! The band that disappears with time corresponds to the $|1\rangle \rightarrow |0\rangle$ transition from the excited to the ground state of the travelling mode. This is merely the decay of thermally populated travelling states upon cooling down the sample. Simultaneously, the band corresponding to the $|0\rangle \rightarrow |1\rangle$ transition is still observed, in accordance with the existence of breathers as parts of the ground state. All these unfounded criticisms reveal a rather superficial examination of experimental data and a lack of realism in applying the quantum sine-Gordon theory to the 4-methylpyridine crystal.

In spite of spectacular successes, the theory proposed for infinite chains of coupled rotors was built with different pieces that may not fit to each other. On the one hand the breather mode is an analytical solution of the sine-Gordon Hamiltonian in Eq. (14). On the other, tunnelling was represented with extended states forming a band structure, according to Eq. (13). However, the tunnelling transitions disappear slowly but undoubtedly with time¹⁴ and this is in conflict with the band structure. These transitions should arise from unstable or metastable species that were not included in the original theory. It is now timely to pursue theoretical models to account for these observations.

5. Conclusions

Tunnelling spectroscopy is unique to observing quantum nonlinear dynamics in crystals and advanced neutron diffraction techniques provide graphic views of the angular probability densities. In addition to these techniques, temperature effects and selective deuteration are necessary to fully determine rotational dynamics. This is a prerequisite to establishing realistic theoretical models. Comparison of methyl rotation in various systems emphasizes the interplay of structures and dynamics and prompt us to elicit existing theories.

In the manganesediacetate tetrahydrate crystal, methyl groups are in three different environments, their rotational axes have different orientations and they are well separated from each other. Methyl groups can be regarded as isolated single rotors.

In the lithiumacetate dihydrate, all methyl groups are equivalent. Close-contact pairs of face-to-face methyl groups with their axis parallel to b

are distributed in (a, b) planes in a nearly hexagonal structure with rather short methyl-methyl distances. The crystal symmetry allows the face-to-face methyl groups to be twisted by 60° and to perform combined rotation. The dynamics of centrosymmetric close contact pairs is well represented with symmetry adapted coordinates. As each methyl group of a pair is surrounded by methyl groups from different pairs there is no collective rotation of the pairs. Methyl-methyl interactions between pairs give rise to an effective potential that depend on the mean angular amplitude of the rotor. For CH_3 rotors, the coupling is rather weak and methyl groups are disordered at any accessible temperature. Only in the deuterated derivative coupling between pairs is strong enough to impose the ordering of the methyl group orientation at low temperature. This is a remarkable example of interplay between dynamics and structure. The symmetry imposes combined rotation of pairs whilst the rotor mass imposes ordering/disordering of the rotors and thus different crystal structures.

In the 4-methylpyridine crystal the distances between methyl groups are quite similar to those in lithiumacetate. However, in the tetragonal structure, there is a conflict between the C_2 local symmetry and the periodicity of the rotors. The face-to-face methyl groups must be twisted by 90° to each other and they cannot perform combined rotation with periodicity less than twelfefold. The corresponding effective potential is virtually a constant. Methyl groups form infinite chains parallel to a or b quite isolated from each other. The collective rotation in 1D is represented with the quantum sine-Gordon theory. There is no phase transition upon methyl deuteration.

References

1. M. Prager and A. Heidemann, *Rotational Tunnelling and Neutron Spectroscopy: A Compilation* (1995).
2. J. R. Durig, S. M. Craven, and W. C. Harris, *Vibrational Spectra and Structure*, vol. 1 p.73 (Marcel Dekker, New York, 1972).
3. W. Press and A. Kollmar, *Solid State Commun.* **17**, 405 (1975).
4. W. Press, *Single particle rotation motion in molecular crystals, Springer tracts in modern physics*, vol. 92 (Springer, Berlin, 1981).
5. S. Clough, A. Heidemann, and M. N. J. Paley, *J. Phys. C: Solid State Phys.* **13**, 4009 (1980).
6. A. Heidemann, H. Fredrich, E. Günther, and W. Häusler, *Z. Phys. B* **76**, 335 (1989).
7. S. Clough, A. Heidemann, A. H. Horsewill, and M. N. J. Paley, *Z. Phys. B* **55**, 1 (1984).
8. A. Heidemann, K. J. Abed, C. J. Barker, and S. Clough, *Z. Phys. B* **11**, 355 (1987).

9. J. Dorignac and S. Flach, Phys. Rev. B **65**, 214305 (2002).
10. L. Soulard, F. Fillaux, G. Braathen, N. L. Calvé, and B. Pasquier, Chem. Phys. Letters **125**, 41 (1986).
11. N. LeCalvé, B. Pasquier, G. Braathen, L. Soulard, and F. Fillaux, J. Phys. C: Solid State Phys. **19**, 6695 (1986).
12. F. Fillaux and C. J. Carlile, Phys. Rev. B **42**, 5990 (1990).
13. F. Fillaux, C. J. Carlile, and G. J. Kearley, Phys. Rev. B **44**, 12280 (1991).
14. F. Fillaux, C. J. Carlile, J. Cook, A. Heidemann, G. J. Kearley, S. Ikeda, and A. Inaba, Physica B **213&214**, 646 (1995).
15. F. Fillaux, G. J. Kearley, and C. J. Carlile, Physica B **226**, 241 (1996).
16. F. Fillaux, C. J. Carlile, and G. J. Kearley, Phys. Rev. B **58**, 11416 (1998).
17. A.-J. Dianoux and G. Lander, *Neutron Data Booklet* (ILL neutrons for science, 2002).
18. M. Neumann and M. R. Johnson, Chem. Phys. **215**, 253 (1997).
19. P. Schiebel, G. J. Kearley, and M. R. Johnson, J. Chem. Phys. **108**, 2375 (1998).
20. J. D. Lewis, T. B. Malloy Jr, T. H. Chao, and J. Laane, J. Mol. Structure **12**, 472 (1972).
21. B. Nicolaï, G. J. Kearley, A. Cousson, W. Paulus, F. Fillaux, F. Gentner, L. Schröder, and D. Watkin, Acta Cryst. B **57**, 3644 (2001).
22. A. Heidemann, S. Clough, P. J. McDonald, A. J. Horsewill, and K. Neumaier, Z. Phys. B **58**, 141 (1985).
23. J. N. van Niekerk and F. R. L. Schoening, Acta Cryst. **6**, 227 (1953).
24. G. M. Brown and R. Chidambaram, Acta Cryst. B **29**, 2393 (1973).
25. E. F. Bertaut, D. T. Qui, P. Burlet, and J. M. Moreau, Acta Cryst. B **30**, 2234 (1974).
26. B. Nicolaï, A. Cousson, and F. Fillaux, unpublished.
27. J. L. Galigné, M. Mouvet, and J. Falgouttes, Acta Cryst. B **26**, 368 (1970).
28. G. J. Kearley, B. Nicolaï, P. G. Radaelli, and F. Fillaux, Solid State Chem. **126**, 184 (1996).
29. P. S. Allen and P. Branson, J. Phys. C: Solid State Phys. **11**, L121 (1978).
30. B. Alefeld, A. Kollmar, and B. A. Dasannacharya, J. Chem. Phys. **63**, 4415 (1975).
31. K. J. Abed, S. Clough, C. J. Carlile, B. Rosi, and R. C. Ward, Chem. Phys. Letters **141**, 215 (1987).
32. N. L. Calvé, D. Cavagnat, and F. Fillaux, Chem. Phys. Letters **146**, 549 (1988).
33. E. K. Morris, Ph.D. thesis, Université d'Orsay (1997).
34. U. Ohms, H. Guth, W. Treutmann, H. Dannohl, A. Schweig, and G. Heger, J. Chem. Phys. **83**, 273 (1985).
35. C. J. Carlile, B. T. M. Willis, R. M. Ibberson, and F. Fillaux, Z. Kristallogr. **193**, 243 (1990).
36. M. A. Neumann, Ph.D. thesis, Université Joseph Fourier, Grenoble, France (1999).
37. C. J. Carlile, S. Clough, A. J. Horsewill, and A. Smith, Chem. Phys. **134**, 437 (1989).
38. G. Voll, Z. Phys. B **90**, 455 (1993).

39. A. Scott, F. Chu, and D. McLaughlin, *IEEE* **61**, 1443 (1973).
40. R. Dashen, B. Hasslacher, and A. Neveu, *Phys. Rev. D* **10**, 4130 (1974).
41. R. Dashen, B. Hasslacher, and A. Neveu, *Phys. Rev. D* **11**, 3424 (1975).
42. S. Coleman, *Phys. Rev. D* **11**, 2088 (1975).
43. M. J. Rice, A. R. Bishop, J. A. Krumhansl, and S. E. Trullinger, *Phys. Rev. Letters* **36**, 432 (1976).
44. R. Jackiw, *Rev. Modern Phys.* **49**, 681 (1977).
45. M. B. Fogel, S. E. Trullinger, A. R. Bishop, and J. A. Krumhansl, *Phys. Rev. B* **15**, 1578 (1977).
46. J. F. Currie, S. E. Trullinger, A. R. Bishop, and J. A. Krumhansl, *Phys. Rev. B* **15**, 5567 (1977).
47. S. E. Trullinger, *Solid State Commun.* **29**, 27 (1979).
48. E. Stoll, T. Schneider, and A. R. Bishop, *Phys. Rev. Letters* **42**, 937 (1979).
49. J. F. Currie, J. A. Krumhansl, A. R. Bishop, and S. E. Trullinger, *Phys. Rev. B* **22**, 477 (1980).
50. R. Rajaraman, *Solitons and instantons. An introduction to solitons and instantons in quantum field theory* (North-Holland, Amsterdam, 1989).
51. Y. S. Kivshar and B. A. Malomed, *Rev. Modern Phys.* **61**, 763 (1989).
52. J. A. D. Wattis, Phd, Mathematics Department, Heriot-Watt University (1993).
53. J. A. D. Wattis, *Physica D* **82**, 333 (1995).
54. A. Scott, *Nonlinear Science. Emergence & Dynamics of Coherent Structures* (Oxford University Press, 1999).
55. R. S. MacKay, in *Nonlinear dynamics and chaos: where do we go from here?* Eds J. Hogan, A. Champneys, B. Krauskopf, M. di Bernardo, M. Homer, E. Wilson and H. Osinga (IOOP, 2002), chap. Many-body quantum mechanics, pp. 100–134.
56. R. S. MacKay and S. Aubry, *Nonlinearity* **7**, 1623 (1994).